Non-Gaussian analysis of diffusion weighted MRI in head and neck cancer: a feasibility study

J. F. Jansen[1], H. E. Stambuk[2], J. A. Koutcher[1], and A. Shukla-Dave[1]

[1]Department of Medical Physics & Radiology, Memorial Sloan-Kettering Cancer Center, New York, NY, United States, [2]Department of Medical Radiology, Memorial Sloan-Kettering Cancer Center, New York, NY, United States

Introduction

Diffusion Weighted Imaging (DWI) allows the measurement of water diffusivity [1]. For head and neck cancer, DWI has mainly been used for characterization [2]. These DWI studies have mainly used 2 to 3 b-factors and mono-exponential fitting to calculate the apparent diffusion coefficient (ADC). However, water in biological structures often displays non-Gaussian diffusion behavior, which has been studied using bi-exponential and kurtosis analysis [3,4]. As a result, the MR signal decay in tissue is not a simple mono-exponential function of the b value [5]. This observation prompts the question whether DWI has the potential of providing information in addition to standard ADC values. The present study investigates the utility of DWI for head and neck cancers in assessing whether non-Gaussian fitting, using the kurtosis model [3], of the diffusion signal decay curves obtained over an extended range of b values may better characterize the tumors than mono-exponential fitting.

Material and Methods

Patients 15 newly diagnosed head and neck cancer patients with metastatic nodes (M/F: 12/3, age: 61±13y, primary cancer: 7 base of tongue, 4 tonsil, 3 nasopharynx, 1 thyroid) underwent a clinical MRI examination. ***MRI*** MRI was performed on a 1.5 Tesla GE Excite scanner using either a 4 or 8-channel neurovascular phased-array coil (phantom experiments assured the feasibility of combining data from both settings). The protocol consisted of MR imaging covering the entire neck or oral cavity/tongue or nasopharynx. DWI images were obtained by using single-shot spin-echo echo-planar imaging. Parameters: TR = 4000 ms, TE = 85-98 ms, averages = 4, slice/gap thickness = 5.0/0 mm, FOV = 20-26 cm, matrix =128x128, and 6 directions, b values: 0, 50, 100, 500, 750, 1000, and 1500 s/mm^2. ***Analysis*** Image processing was performed using Matlab and SPM5. For all of the 6 DWI images with a b-value > 0 s/mm^2, a corresponding image with b=0 s/mm^2 was obtained. All 6 b=0 images were aligned using affine transformation in SPM5. All corresponding DWI images with b > 0 s/mm^2 were transformed using these parameters. An averaged b=0 image was obtained after realignment. Gaussian smoothing was applied on all images with a FWHM of 3 mm. Masks were created on the averaged b=0 image using MRIcro, to select regions of interest (ROI) of the primary tumors, nodes and spinal cord. Fits were performed on a voxel-by-voxel basis with a Marquardt-Levenberg algorithm, using: $\ln[S(b)]=\ln[S(0)]-b\cdot D_{app}+1/6\cdot b^2\cdot D_{app}^2\cdot K_{app}$, where S is the signal intensity, b is the b value (s/mm^2), D_{app} is the apparent diffusion coefficient (10^{-3}mm^2/s), and K_{app} is the apparent kurtosis coefficient [6]. In addition to non Gaussian fitting, mono-exponential fitting was performed using (K_{app}=0, yielding ADCmono). To determine whether the non Gaussian model provided a statistically improved fit over the mono-exponential model, the two models were tested using an F-test (P <0.05).

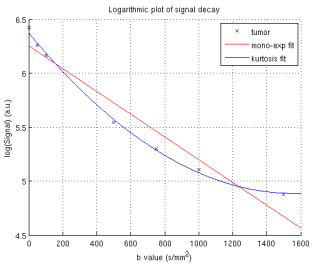

Figure 1 Logarithm of the averaged MR signal decay of the right node of patient 9 as function of b value.

Results

Mean ADCmono, D_{app}, and K_{app} values for various regions are given in table 1. ADCmono values are in agreement with the literature [2]. In figure 1 a typical example is given of the signal decay curve and fits of mean intensity as function of b value of a lymph node of patient 9 (M 62y, primary cancer: base of tongue). The non Gaussian kurtosis analysis fits the data points substantially better, confirmed by an F-test. For all individual cases of the whole population, the non Gaussian kurtosis analysis was always significantly better than the mono-exponential fit (P <0.05). Figure 2 shows the MRI image series obtained from the oral cavity of patient 9. From the STIR image in 2b, it can be observed that both the nodes were of heterogeneous nature. Fitted results from the right node are shown in Figure 2e-h by using a mask overlay on the realigned mean b=0 image. The heterogeneity for the right node is not clear in 2(e), the ADCmono map, but it can be easily observed in the images from D_{app} (2f) and K_{app} (2g). To evaluate this potential added value of the non Gaussian kurtosis analysis, for all voxels of the right node highlighted in figure 2e, the D_{app} was plotted as function of the K_{app} (figure 3). The Spearman rank-order correlation coefficient for this case was -0.34, indicative of a weak correlation between the K_{app} and D_{app}. This suggests that K_{app} provides additional information on the water diffusion properties. The range of Spearmans rho for all lesions of the population was -0.2 to -0.9, for 60% of the lesions it ranged between -0.2 and -0.5.

Region (n)	ADCmono	Dapp	Kapp
Node (21)	0.89 ± 0.26	1.58 ± 0.49	1.32 ± 0.37
BOT (7)	0.74 ± 0.14	1.55 ± 0.27	1.50 ± 0.27
Tonsil (4)	0.97 ± 0.07	1.86 ± 0.27	1.12 ± 0.12
Nasopharynx (2)	0.59 ± 0.26	1.02 ± 0.37	2.02 ± 0.94
Spinal cord (11)	0.77 ± 0.12	1.41 ± 0.30	1.33 ± 0.19

Table 1 Average results of calculated DWI values (mean ± SD)

Discussion

The choice of b-values has a great impact on the magnitude of the ADC values, especially when calculated using a mono-exponential approach. Previously, Thoeny et al. found that DWI using low b-values generally yields higher ADC values than DWI using high b-values in mon-exponential fit [7]. There is substantial evidence that the diffusion decay is of non-mono exponential origin, however the exact nature of this behavior is not well understood [3]. Studies in brain and prostate have used non mono-expeonential fitting (bi-exponential or kurtosis) and have found that it is better than the mono-exponential fit [3,4,6]. We have used the kurtosis analysis which incorporates non-Gaussian diffusion without any assumptions on the nature of multiple compartments contrary to bi-exponential fitting. The assumptions in compartmental analysis have their own limitations [4,6]. We found that, although K_{app} is not necessarily independent of D_{app} for all tumors, 60% of the tumors had low correlation. The advantage of this data being that it is a specific measure of tissue structure. Therefore, we believe that the diffusional kurtosis model yields a parameter (K_{app}) that might be more sensitive to pathological changes, even when the exact nature is yet to be fully understood. The ADC estimated using the mono-exponential model is systematically lower than D_{app} from the difussional kurtosis model. This is in agreement with earlier findings in brain by Lu et al [6], who attributed this discrepancy to the nature of the diffusional kurtosis model. A second-order polynomial fitting model (kurtosis) will always give better fitting results than a linear model. Therefore, the non-Gaussian kurtosis model can provide a more accurate estimation of the ADC than the mono-exponential model.

Conclusion

The diffusional non Gaussian (kurtosis) model provides a significantly better fit for DWI in head and neck cancer acquired over an extended b-value range. Furthermore, it yields a better estimation of a more accurate ADC (D_{app}), and provides an additional parameter, K_{app}, potentially with added value. This may be of importance as accurate ADC values are needed for clinical purposes especially in longitudinal studies.

References

[1] Koh, AJR Am J Roentgenol 2007 188:1622; [2] Maeda, J Neuroradiol 2008 35:71; [3] Jensen, Magn Reson Med 2005 53:1432; [4] Shinmoto, MRI 2008; [5] Karger, Adv Colloid Interface Sci 1985 23:129; [6] Lu, NMR Biomed 2006 19:236; [7] Thoeny, JMRI 2006 20:786.

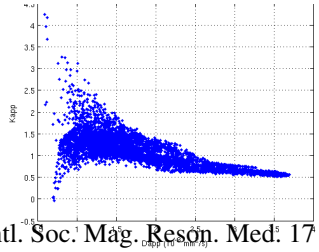

Figure 3 Scatter plot showing the correlation between the Dapp and the Kapp obtained from the diffusional kurtosis analysis. Spearman's rho = -0.34

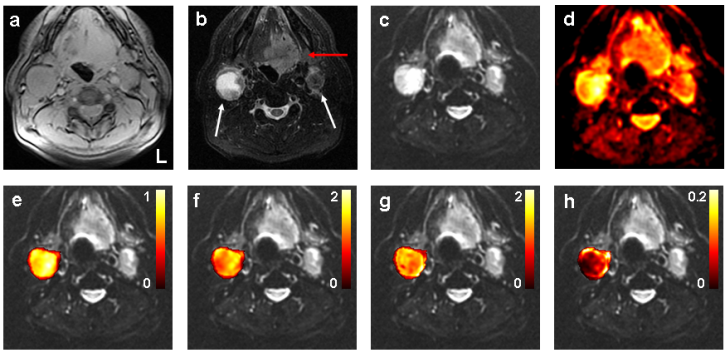

Figure 2 Axial MRI images from the oral cavity of patient 9. (a) PD image, (b) T2 STIR image, (c) realigned mean b=0 image, (d) ADCmono map. The second white arrows in (b) indicate the primary tumor and metastatic nodes, respectively. Figures (e-f) display pixel-by-pixel calculation outcomes for the right node. (e) ADCmono (10^{-3} mm^2/s). (f) Dapp (10^{-3} mm^2/s), (g) Kapp, and (h) chi^2.